DOI 10.31489/2023NO2/118-126

UDC 539; 535.37

ENHANCING PHOTOMETRIC PERFORMANCE OF YAG:Ce CERAMICS: INVESTIGATING THE ROLE OF ANNEALING IN RADIATION-ASSISTED SYNTHESIS

Zhilgildinov Zh.S.[1], Lisitsyn V.M.[2], Karipbayev Zh.T.[1*], Tulegenova A.T.[3], Alpyssova G.K.[4*], Mussakhanov D.A.[1], Zhunusbekov A.M.1[1]

[1]L.N. Gumilyov Eurasian National University, Astana, Kazakhstan, karipbayev_zht_1@enu.kz

[2]National Tomsk Polytechnic University, Tomsk, Russia

[3]Al-Farabi Kazakh National University, Almaty, Kazakhstan

[4]E.A Buketov University, Karaganda, Kazakhstan gulnur-0909@mail.ru

Ceramic samples of cerium-doped yttrium aluminum garnet (YAG:Ce) were successfully synthesized utilizing a high-powered electron flux field with a considerable energy level of 1.4 MeV and a power density of 23 kW/cm2. The ceramics were formed in a remarkable time span of just one second from a specifically prepared mix of yttrium, aluminum, and cerium oxides. The process of radiation-assisted synthesis of ceramics within radiation flux fields fundamentally deviates from the methodologies commonly employed today. Analyzed diffraction patterns closely align with those documented for YAG:Ce crystals, both in peak position and proportion. Furthermore, every sample consistently demonstrated a space group symmetry of Ia-3d. The luminescence and excitation spectra of ceramics synthesized in this study closely resemble those of YAG:Ce ceramics produced by other methods and YAG:Ce - based phosphors. The luminescence bands exhibit high efficiency, and the intensity ratios of the UV bands vary among the studied phosphors. The ceramics' radiation-to-luminescence conversion efficiency was found to be impressive, achieving scores of 0.57 and 0.48 in the industrial phosphors SDL 4000 and YAG-02, respectively. It was also observed that an increase in quantum efficiency of the samples could be achieved via high-temperature annealing. High conversion efficiency underscores the potential of the outlined luminescent ceramics synthesis method.

Keywords: synthesis, YAG:Ce ceramics, structure, radiation-assisted synthesis, luminescence.

Introduction

Phosphor materials play a crucial role in various modern technologies, particularly in the fields of lighting and display systems. These materials possess the unique ability to convert energy from one form into another, most commonly transforming ultraviolet (UV) or high-energy visible light into lower-energy visible light [1-4] Among the numerous phosphor materials available, Ce^{3+} - doped luminescent phosphors have emerged as a promising candidate for a range of applications [5-10]. In particular, cerium-doped yttrium aluminum garnet (YAG:Ce) phosphor ceramics are innovative materials that evolve from the base compound of YAG, doped with cerium (Ce) ions. This insightful fusion results in an exceptional transformation of the YAG crystal structure, thereby birthing a highly efficient phosphor material that boasts distinct optical properties.

Notably, the luminescent characteristics of YAG:Ce phosphor ceramics can be deliberately customized. This is achieved by expertly manipulating certain aspects of the synthesis process, as well as the relative concentrations of the cerium dopant. By making these strategic alterations, the optical properties of the resultant ceramic material can be attuned to cater to a plethora of specific application requirements.

Such versatility and customizability empower these phosphor ceramics to function in a wide range of sectors. From lighting technologies to imaging devices, from signal amplification in telecommunications to their application in medical imaging, the YAG:Ce phosphor ceramics, with their unique properties, can be fine-tuned to meet diverse requirements, reinforcing their appeal and utility in numerous technological innovations [10]. YAG:Ce based phosphor ceramics demonstrate promising potential for applications in light-emitting diodes (LEDs)[11-13] and scintillators[14-16]. These multicomponent systems often require high-temperature and lengthy synthesis processes, which can result in inconsistent material quality. Consequently, ongoing research is focused on refining and discovering new synthesis techniques. The

growing interest in YAG:Ce phosphor ceramics is primarily driven by their potential use in energy-efficient lighting technologies, such as light-emitting diodes (LEDs). The exceptional conversion efficiency, thermal stability, and color-rendering properties of YAG:Ce phosphor ceramics make them an ideal choice for the generation of white light in LEDs.

Apart from widely-used solid-phase reactions [13], various alternative methods are being explored, such as laser ablation [17], sol-gel [18], hydrothermal [19], coprecipitation [20], and combustion [21]. One promising approach involves synthesizing ceramics within high-power radiation fluxes. Studies have demonstrated that MgF2-based luminescent ceramics can be synthesized using high-power electron fluxes [22], and we previously showed that YAG:Ce ceramics can also be synthesized in this manner[23]. The spherical ceramic samples obtained, up to 7mm in size, exhibited luminescence upon UV excitation in the spectral region characteristic of YAG:Ce phosphor ceramics.

This paper presents the results of synthesizing YAG:Ce ceramics radiation-assisted method, along with an analysis of the material's structural and luminescent properties.

1 Materials and Research Methods

The synthesized test samples were two series of ceramics different in composition with a batch content: Y_2O_3(55%) + Al_2O_3(43%) + Ce_2O_3(2%) (YAG) and Y_2O_3(52%) + Al_2O_3(40%) + Ce_2O_3(2%) + Gd_2O_3(6%) (YAG:Ce, Gd). The initial experimental outcomes reveal that the synthesis of YAG:Ce ceramics within a radiation-assisted method is heavily influenced by the precursor prehistory of the components used in the synthesis process. Particularly, the history of the aluminum oxide powders employed exerts significant impact on the synthesis results.

Given this key finding, we chose to utilize three distinct types of alumina powders procured from different suppliers to ascertain the synthesis variance. These powders were sourced from Hefei Zhonghang Nanotechnology Development Co. Ltd. in China, marked as A with the product specification ZH-Al2O3-01; Labor Farma in Kazakhstan, denoted as B and classified under ChDA TU 6-09-426-75; and lastly, Chemical Reagents Plant in Russia, labelled as C and also conforming to the qualification ChDA TU 6-09-426-75.

It is important to note that the constituent dispersion of these powders was varied, leading to different experimental conditions and thereby potentially impacting the synthesis outcomes of the YAG:Ce ceramics. Hereafter, phosphors of two series (YAG and YAG:Ce, Gd) made using alumina of different prehistory are indicated by numbers in accordance with Table 1.

Table 1. Designation of ceramic samples

	Sample No.	Composition	Manufacturer Al_2O_3
YAG:Ce	1	Al_2O_3 (43%) + Y_2O_3(55%) + Ce_2O_3(2%)	A
	2	Al_2O_3 (43%) + Y_2O_3(55%) + Ce_2O_3(2%)	B
	3	Al_2O_3 (43%) + Y_2O_3(55%) + Ce_2O_3(2%)	C
YAG:Ce, Gd	4	Al_2O_3 (40%) + Y_2O_3(52%) + Ce_2O_3(2%) + Gd_2O_3(6%)	A
	5	Al_2O_3 (40%) + Y_2O_3(52%) + Ce_2O_3(2%) + Gd_2O_3(6%)	B
	6	Al_2O_3 (40%) + Y_2O_3(52%) + Ce_2O_3(2%) + Gd_2O_3(6%)	C

Oxide powder samples were sintered using high-power electron flux to form YAG:Ce phosphor ceramics. Stoichiometric powders were poured into a 5mm-deep copper crucible with an area of up to 40x120 mm^2. The crucible was exposed to a high-intensity electron flux that was transmitted from a vacuum state to atmospheric pressure via a differential vacuum pumping system. This electron flux was generated by the ELV-6 accelerator, housed at the Institute of Nuclear Physics of the Siberian Branch of the Russian Academy of Sciences (INP SB RAS). The electron flux carried a substantial energy of 1.4 MeV and had a power density of 23 kW/cm^2. An electron beams systematically scanned the surface of the powder held within the crucible, moving at a steady speed of 1 cm/s. The cross-sectional density of the electron beam displayed a Gaussian distribution and had a diameter measuring 7 mm at its proximity to the charge surface.

This scanning process ensured that every point on the surface of the crucible was evenly exposed to the electron flux for a duration of 1 second, allowing for a controlled and systematic experiment. After exposure,

the mixture rapidly solidified, forming ceramic samples that were plate-like or spherical in shape. Up to 10 different-sized samples were formed in each crucible. After a single irradiation, the crucible was cooled, and the samples were removed. The samples were then annealed at a temperature of 1650°C for 8 hours. This article presents the research conducted before and after the annealing process.

The luminescence quantum yield (QE) of the synthesized ceramics was measured using an FLS1000 PL spectrometer (Edinburgh) and an integrating sphere (120mm diameter) in the 250-870 nm range. QE measurement involved two stages: 1) measuring the scattered radiation (i.e., outgoing radiation) and the radiation range of the empty integrating sphere; 2) repeating the measurements with the sample placed inside the sphere. The program calculated the QE from the received data. The samples were excited at 450 nm, with a calculation range for QE of 438.5 - 461.8 nm (excitation) and 467.9 - 740.0 nm (luminescence). QE measurements were taken from both the inner and outer sides of the annealed and unannealed samples. The samples exhibited a porous inner surface and a smooth outer surface.

2 Results and discussion

The synthesized samples included plate-like structures with diameters up to 3 cm and thicknesses of around 3 mm, as well as spherical cavities ranging in diameter from 0.5 to 1.5 cm with wall thicknesses of approximately 1.5 mm. These cavities were filled with porous ceramics. Images of samples 2 and 4 are presented in Figure 1. The color of the synthesized samples varied from yellow-green to yellow, depending on the history of the alumina powders used. These samples were fragile, prone to cracking upon impact, and exhibited hardness levels comparable to corundum. Refer to Figure 1 for photographs of the samples.

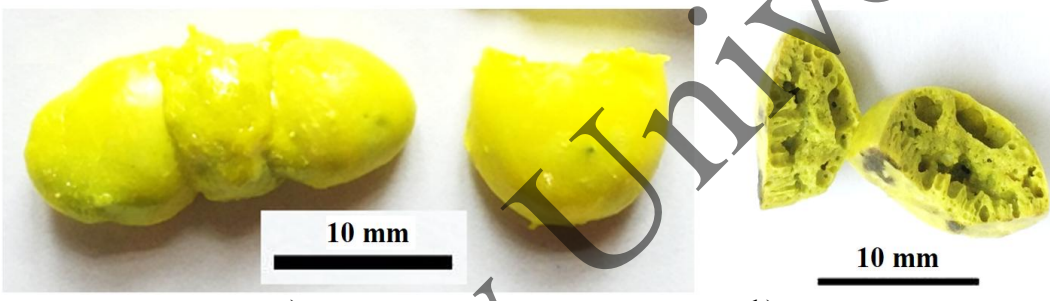

a) b)

Fig. 1. Photographs of ceramic sample 2 (a- inside, b- outside).

For the study, ceramic samples were mechanically ground into particles with sizes smaller than 1 mm. Figure 2 presents photographs of sample 4, captured using a microscope after exposure to chip radiation at λ=450 nm and illumination from an incandescent lamp, along with images taken by an MD300 digital camera.

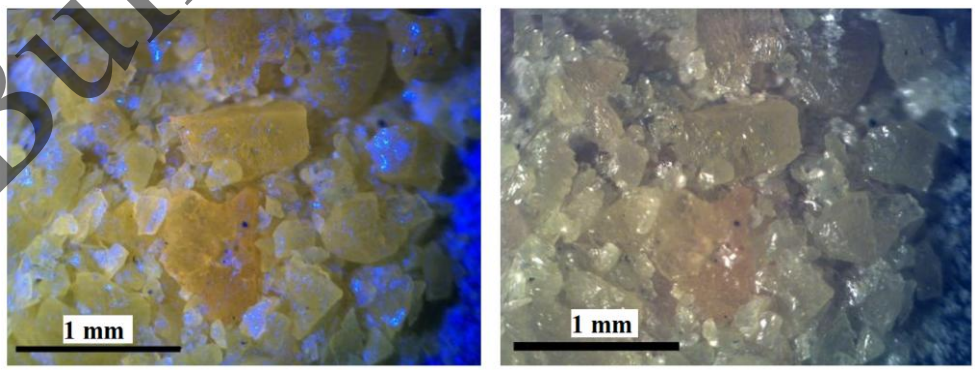

a) b)

Fig. 2. Photograph of the powder prepared from sample 4 exposed to chip radiation with λ=450 nm (a) and an incandescent lamp (b).

Exposure to chip radiation resulted in intense luminescence in the yellow region, with a portion of the chip radiation scattering on cleavage planes. Some particles displayed flat, cleaved boundaries, suggesting a tendency towards crystalline structure formation. The sample morphology was examined utilizing a Quanta3D 200i scanning electron microscope (SEM) manufactured by FEI Company in the USA. In Figure 3, SEM images displaying the cleavage site for YAG:Ce and Gd (sample 4) are presented.

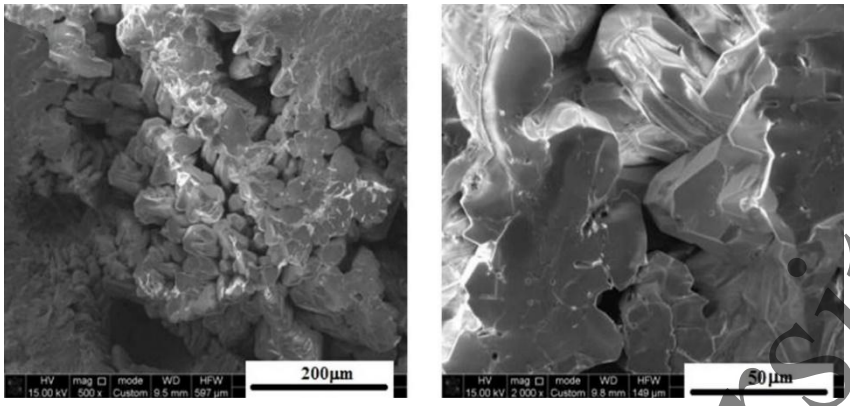

a) b)

Fig 3. SEM images of the cleavage site for sample 4 (YAG:Ce, Gd) at different magnification

SEM images of the cleavages show that ceramic samples are soldered particles with sizes of ~10...50 µm. Most of the particles are in the form of melt. Particles with a well-defined faceting observed indicate the formation of microcrystals. To analyze the structure of the synthesized YAG:Ce and YAG:Ce, Gd ceramics, a Rigaku Miniflex 600 X-ray diffractometer was employed. The resulting data were then compared with ICSD standards, specifically PDF-2 Release 2016 RDB 00-066-0538 (YAG) and PDF-2 Release 2016 RDB 00-06-0291 (YAG:Ce, Gd). Figure 4 showcases the XRD measurement outcomes for YAG:Ce and YAG:Ce, Gd, displaying the XRD patterns for phosphors 2 and 5. The spectra indicate the positions of the spectral lines.

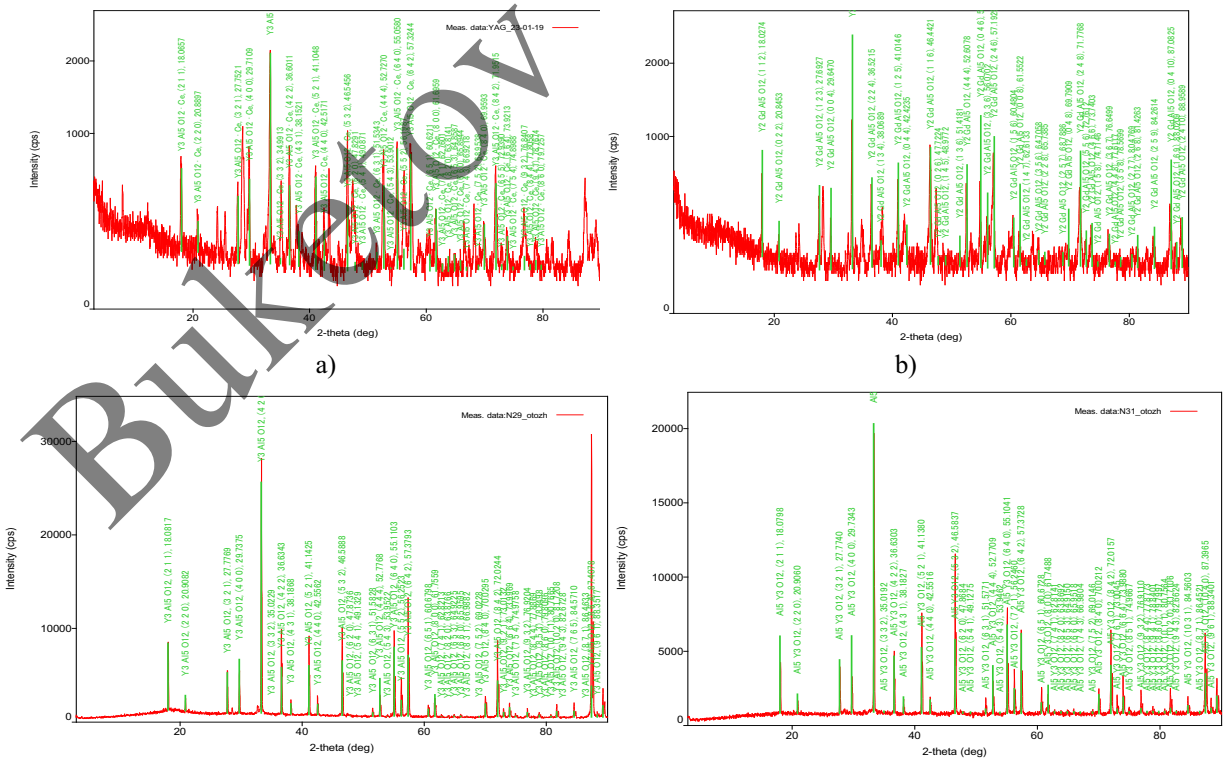

a) b)

c) d)

Fig. 4. XRD spectra for before annealing – YAG:Ce (a) and YAG:Ce, Gd (b), after annealing YAG (c) and YAG:Ce, Gd (d) ceramic powders

The size of crystallites is often determined using X-ray diffraction (XRD) through the Scherrer equation. This method computes crystallite sizes based on the full width at half maximum (FWHM) of the diffraction peak, the wavelength of the X-ray radiation used, and the Bragg angle. Following the synthesis of ceramics under the influence of intense radiation flux, the samples typically exhibit an inherent level of defects. Subjecting these samples to high-temperature annealing decreases defect density while enhancing crystallinity.

This improvement is mirrored in the parameters of the crystal structure, which draw closer to their standard values. The study, however, does not prioritize providing numerical evaluations of structural distortions. Additional data on the structure of ceramic samples are presented in Table 2.

Table 2. Parameters of the crystal lattice and crystallites of YAG:Ce and YAG:Ce, Gd phosphors

Sample	Compound	Lattice parameters (a,b,c), A^o	Crystallite size (nm)		
		before annealing	after annealing	before annealing	after annealing
YAG: Ce	(Al_2O_3 (43%) + Y_2O_3(55%) + Ce_2O_3(2%)	a=12.0234 b=12.0234 c=12.0234	a=12.007477 b=12.007477 c=12.007477	47.24	92.7
YAG: Ce, Gd	Al_2O_3 (40%) + Y_2O_3(52%) + Ce_2O_3(2%) +Gd_2O_3(6%)	a=12.0546 b=12.0546 c=12.0546	a=12.008721 b=12.008721 c=12.008721	81.32	116.7
YAG (ICSD)	$Y_3Al_5O_{12}$	a=12.0062 b=12.0062 c=12.0062	Unit Cell Data Source: Single Crystal.		

The diffraction patterns presented in Figure 4 correspond closely to the known positions and peak ratios associated with YAG:Ce crystals. It's evident that all samples demonstrate characteristics of the Ia-3d space symmetry group. As shown in Table 2, the substitution of Ce^{3+} ions with Gd^{3+} ions result in an increase in the lattice parameter by 0.031 Å. The enlargement of the average lattice parameter due to Gd^{3+} incorporation leads to a red shift in the luminescence band caused by Ce^{3+} ions [24]. High-temperature annealing demonstrates better conformity with the YAG standard (Space group: 230: Ia-3d; Phase: $Y_3Al_5O_{12}$, in accordance with the ICDD data sheet (PDF-2 Release 2016 RDB) – 230: Ia-3d) and enhanced crystallinity of the ceramics, as seen in Figure 4 (c) and (d).

3 Luminescent properties of synthesized ceramics

PLspectra of the phosphors were measured using Agilent Cary Eclipse and Solar CM2203 fluorescence spectrophotometers. Figure 5 presents the luminescence spectra results for the ceramic samples when excited at 450, 340, and 270 nm wavelengths. The spectrum shape remains consistent regardless of the excitation wavelength (a and b). Two broad luminescence bands at 520 and 580 nm are attributed to the $^5D_0 \rightarrow {}^4F_{5/2}$, $^4F_{7/2}$ transitions [25]. The luminescence and excitation spectra of ceramics synthesized in this study closely resemble those of YAG:Ce ceramics produced by other methods [26-27] and YAG:Ce-based phosphors [27-30].

When samples are excited by radiation at 270 nm, additional luminescence is observed in the UV spectral region, with bands at approximately 320, 370, and 415 nm. These bands can also be detected in commercial phosphors [31] under the same excitation conditions. The UV luminescence bands exhibit high efficiency, and the intensity ratios of the UV bands vary among the studied phosphors. Figure 5d depicts the locations of the luminescence band maxima for all the samples studied under excitation in the region of 450 nm.

Interestingly, the luminescence band maxima positions in the Gd^{3+}-enriched phosphors (samples 4-6) tend to shift toward the long-wavelength spectral area, as compared to phosphors 1-3. This trend is consistent with the well-established understanding regarding the influence of the modifier [24]. It's worth highlighting that the overall shape of the luminescence spectra in the range of 480-700 nm remains unaffected by the method of excitation.

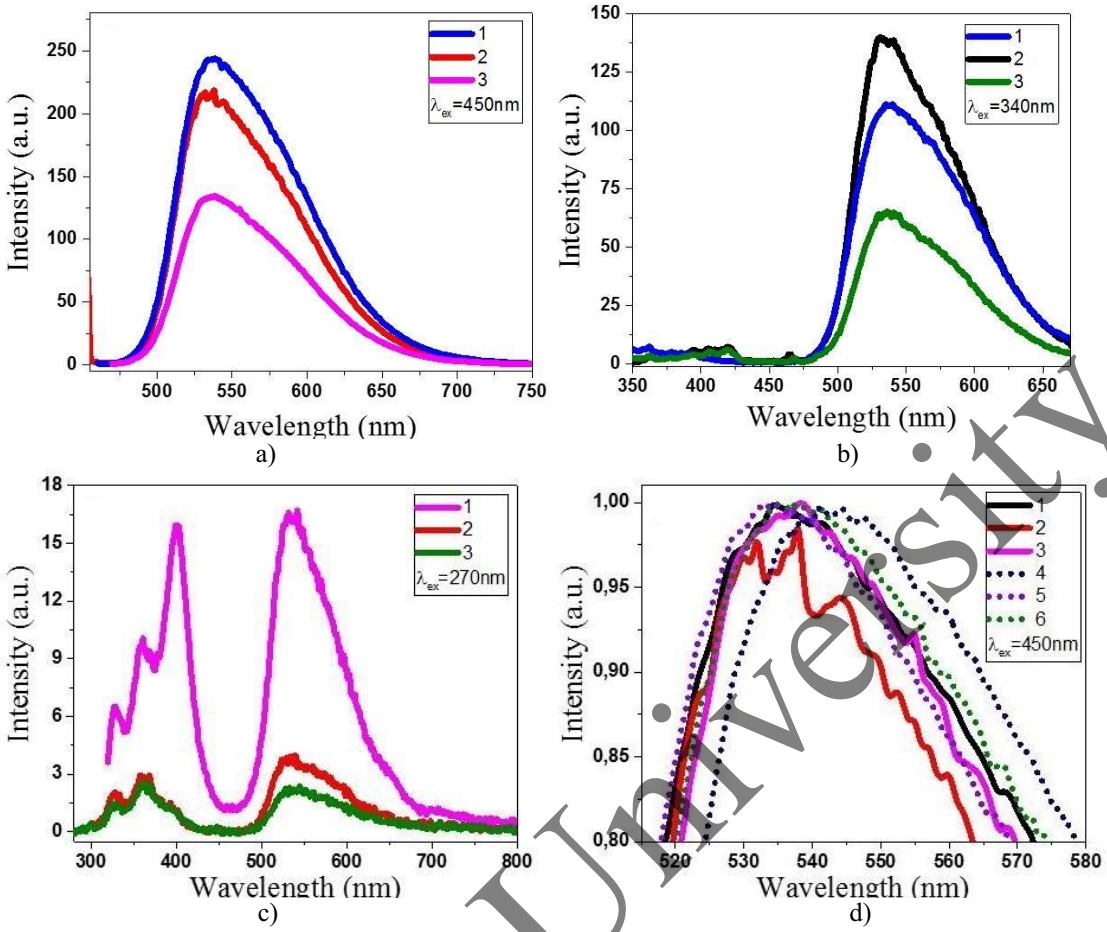

Fig 5. Luminescence spectra of the synthesized samples upon excitation at:
a) 450 nm, b) 340 nm, c) 270 nm, d) 450 nm.

The luminescence spectra obtained from the pulverized samples of the synthesized ceramics, when excited by chip radiation at 450 nm and 365 nm, as well as by a laser of 337 nm wavelength measured using an AvaSpec-2048 spectrophotometer, are fundamentally consistent with those illustrated in Figure 5. Figure 6 showcases the outcomes of luminescence spectrum measurements for synthesized samples 1-3 under 540 nm excitation. The form of these excitation spectra is notably characteristic of YAG:Ce phosphors. The emergence of two excitation bands for Ce^{3+} at 460 nm and 340 nm are a consequence of the $^4F_{5/2} \rightarrow {}^5D_0$ and $^5D_1$ transitions, respectively [27].

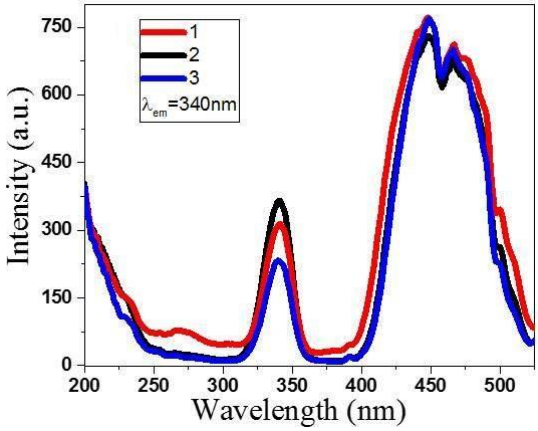

Fig. 6. Luminescence spectra of the synthesized samples excited in the region of 540 nm measured before (a) and after (b) high-temperature annealing.

Effective luminescence can also be excited by radiation with wavelengths shorter than 300 nm. As the wavelength decreases, luminescence steadily increases in the 550 nm region. When excited by 450 nm laser pulses, a nanosecond component prevails in the luminescence decay kinetics in the 550 nm region. Its characteristic time spans from 56 to 60 ns in samples 1, 2, 4, and 5. In samples 3 and 6, the characteristic time ranges from 40 to 52 ns. During these periods, the luminescence intensity decreases by two orders of magnitude within 300 ns. The nanosecond decay component is a distinctive feature of photoluminescence in YAG:Ce phosphors. In order to expediently ascertain the radiation-to-luminescence conversion efficiency, we employed a specific method. By maintaining a constant spatial relationship between the excitation source and the phosphor, we can infer that the conversion efficiency is directly proportional to the observed brightness. When dealing with a luminous object exhibiting a Lambertian distribution (L), its brightness is directly connected to luminosity (M) and the light flux projected into the hemisphere (Fv), as described by the following relationships:

$$F_v = MS = 2\pi LS \quad (1)$$

where S is the luminous surface area. The surface area of the phosphor, whose luminance is being gauged, is determined by the brightness meter's telescopic system and remains consistent throughout the measurement process.

There exists a relationship between the radiation flux (Fe) and the light flux (Fv) emanating from the phosphor, as expressed by the following equation:

$$F_e = F_v \frac{1}{683} \frac{\int_0^\infty \varphi(\lambda) d\lambda}{\int_0^\infty v(\lambda)\varphi(\lambda) d\lambda} \quad (2)$$

For phosphors of the same type, for example, YAG:Ce, we can assume that their radiation spectra φ(λ) are similar. In this case, the ratio of the radiation fluxes Fv1 and Fv2 of sources with similar emission spectra: $\varphi_1(\lambda) = \varphi_2(\lambda)$, the Lambertian distribution of luminance and equal luminous surface areas, is equal to:

$$\frac{F_{e1}}{F_{e2}} = \frac{F_{v1}}{F_{v2}} = \frac{M_1 S}{M_2 S} = \frac{L_1}{L_2} \quad (3)$$

Hence, for a specific system of phosphors with analogous emission spectrums (φ1(λ)=φ2(λ)), there exists a direct proportionality between the radiation flux and the luminance. Given a stable spatial configuration of the measurement system components, which includes the excitation source, the phosphor, and the brightness meter, the ratio of brightness corresponds to the ratio of efficiencies in the radiation-to-luminescence conversion. Brightness evaluations were performed utilizing a CS-200 Chroma meter. Commercial phosphors SDL 4000 (from NPO Platan, Russia) and YAG 02 (from GrandLux Optoelectronic Co. Intematix Corporation, PRC), with their attributes detailed in [30], served as reference samples for brightness measurement, and thereby, the calculation of phosphor efficiency. Luminescence was excited by LED radiation with a wavelength of 450 nm. Measurements were conducted for powdered ceramic samples and industrial phosphors placed in washers, with the spatial location of the stand components remaining constant during measurements. No specific pattern was observed regarding the impact of high-temperature annealing on the brightness of ceramics. The outcomes of the measurements are showcased in Table 3.

Table 3. Measurement results for brightness L of the synthesized phosphors upon excitation with λ_{ex}= 450 nm.

Sample number	L, cd/m^2 λ_{ex}=450	
	before annealing	after annealing
1	201	193
2	143	179
3	201	235
4	205	176
5	160	188
6	188	200
SDL 4000 (Reference)	360	
YAG – 02 (Reference)	422	

The data shows that brightness of the synthesized phosphors is approximately twice lower than that of industrial phosphors. High temperature annealing increases QE of samples. The Table 4 provides data on the brightness observed for commercial reference phosphors.

Table 4. Brightness of reference phosphors

Sample number		QE, %	
		before annealing	after annealing
2	inside	25.8	35.6
	outside	24.20	43.7
6	inside	37.70	39.4
	outside	39.2	56.1
SDL 4000 [23]		40.4	

Conclusions

The study results indicate that high-power fluxes of hard radiation can be employed for synthesizing YAG:Ce-based ceramics. Activated Ce^{3+} and modified Gd^{3+} ceramics with sizes up to 1.5 cm^3 were produced. XRD analysis revealed a YAG:Ce crystalline phase in samples 1-3 and an additional YAG:Ce, Gd phase in samples 4-6. The properties of the radiation-assisted synthesized samples bear a striking resemblance to those of ceramics. The spectral-kinetic properties of luminescence and excitation found in ceramics, correspond closely to those seen in YAG:Ce and YAG:Ce, Gd phosphors produced using traditional techniques. The conversion efficiency from radiation to luminescence is notably high, attaining values of 0.48 and 0.57 in the reference commercial phosphors YAG-02 and SDL 4000, respectively. This high conversion efficiency underscores the potential of the outlined luminescent ceramics synthesis method.

It's significant to highlight the broad spectrum of conversion efficiencies observed in samples with diverse precursor histories, especially those involving aluminum oxides of varying sources. To enhance the production of ceramics exhibiting high emissive qualities, future research should explore the correlation between luminescent properties and factors such as precursor quality, dopant concentration, modifier, pre-treatment of the mixture, among others.

The process of radiation-assisted synthesis of ceramics fundamentally deviates from the methodologies commonly employed today. This process is governed not solely by temperature, but also by a high ionization density. The irradiation modes used result in an energy output of 11×10^{23} eV/cm^3 during a 1-second exposure to the flux. The generation of one electronic excitation under intense radiation necessitates energy corresponding to 2-3 band gap energy. Consequently, throughout the synthesis duration, approximately 5.5×10^{22} cm^{-3} electronic excitations (which include electrons, holes, and electron-hole pairs) are produced within 1 cm3 of the materials employed (Y_2O_3, Al_2O_3, Gd_2O_3, Ce_2O_3), which possess an average band gap of 10 eV. The decay of electronic excitation generates intermediate radiolysis products – radicals with a lifetime of around 10^{-6} s, which significantly increase the efficiency of solid-state reactions and enhance mixing of the batch components. At this level of electronic excitation density, reaction efficiency between charged components is considerably higher than solid-phase synthesis.

Acknowledgments

This research has been funded by the Science Committee of the Ministry of Education and Science of the Republic of Kazakhstan (Grant No. AP14870696).

This research has been funded by the Russian Science Foundation of the Russian Federation. (Grant No. 23-73-00108).

REFERENCES

1 Ueda J., Tanabe S. Review of luminescent properties of Ce3+-doped garnet phosphors: New insight into the effect of crystal and electronic structure. *Optical Materials,* 2019. Vol.1. pp. 100018. doi:10.1016/j.omx.2019.100018

2 Pankratov V., Popov A.I., Shirmane L., et al. Luminescence and ultraviolet excitation spectroscopy of SrI2 and SrI2:Eu^{2+}. *Radiation Measurements*, 2013. Vol. 56, pp. 13-17. doi:10.1016/j.radmeas.2013.02.022

3 Chernov S.A., Trinkler L., Popov A.I. Photo- and thermo-stimulated luminescence of CsI-Tl crystal after UV light irradiation at 80 K. *Radiation Effects and Defects in Solids*, 1998. Vol. 143 (4), pp. 345-355. doi:10.1080/10420159808214037

4 Elsts E., Rogulis U., Bulindzs K., et al. Studies of radiation defects in cerium, europium and terbium activated oxyfluoride glasses and glass ceramics. *Optical Materials,* 2015. Vol. 41, pp. 90-93. doi:10.1016/j.optmat.2014.10.042

5 Pankratov V., Popov A.I., Kotlov A., Feldmann C. Luminescence of nano- and macrosized $LaPO_4$:Ce,Tb excited by synchrotron radiation. *Optical Materials*, 2011. Vol.33 (7), pp. 1102-1105. doi:10.1016/j.optmat.2010.12.019

6 Polisadova E., Valiev D., Vaganov V., et al. Time-resolved cathodoluminescence spectroscopy of YAG and YAG:Ce^{3+} phosphors. *Optical Materials,* 2019. Vol. 96, pp. 109289. doi:10.1016/j.optmat.2019.109289

7 Karipbayev Z.T., Lisitsyn V.M., Mussakhanov D.A., et al. Time-resolved luminescence of YAG:Ce and YAGG:Ce ceramics prepared by electron beam assisted synthesis. *Nuclear Instruments and Methods in Physics Research, Section B: Beam Interactions with Materials and Atoms*, 2020. Vol. 479, pp. 222-228. doi:10.1016/j.nimb.2020.06.046

8 Sidorenko A.V., Bos A.J.J., Dorenbos P., et al. Storage properties of Ce^{3+} doped haloborate phosphors enriched with^{10}B isotope. *Journal of Applied Physics,* 2004, Vol. 95 (12), pp. 7898-7902. doi:10.1063/1.1719260

9 Platonenko A., Popov A.I. Structural and electronic properties of β-NaYF4 and β-NaYF4:Ce^{3+}. *Optical Materials*, 2020. Vol. 99, pp. 109529. doi:10.1016/j.optmat.2019.109529

10 Karipbayev Z.T.; Lisitsyn V.M.; Golkovski M.G.; Zhilgildinov Z.S., et al. Electron Beam-Assisted Synthesis of YAG:Ce Ceramics. *Materials*, 2023. Vol. 16, pp. 1-11. doi:10.3390/ma16114102

11 Narukawa Y., Ichikawa M., Sanga D., Sano M., Mukai T. White light emitting diodes with super-high luminous efficacy. *J. Phys. D Appl. Phys.*, 2010. Vol.43, pp. 354002. doi:10.1088/0022-3727/43/35/354002

12 George N.C., Denault K.A., Seshadri R. Phosphors for solid-state white lighting. *Annu. Rev. Mater. Res.,* 2013,Vol. 43, pp. 481–501. doi:10.1146/annurev-matsci-073012-125702

13 Ye S., Xiao F., Pan Y.X., et al. Phosphors in phosphor-converted white light-emitting diodes: Recent advances in materials, techniques and properties. *Mater. Sci. Eng. R Rep.,* 2010, Vol.71, pp. 1–34. doi:10.1016/j.mser.2010.07.001

14 Yoshikawa A., et al. Crystal growth and scintillation properties of multi-component oxide single crystals: Ce:GGAG and Ce:La-GPS. *J. Lumin.,* 2016, Vol.169, pp. 387–393. doi:10.1016/j.jlumin.2015.04.001

15 Osipov V.V., Ishchenko A.V., Shitov V.A., et al. Fabrication, optical and scintillation properties of transparent YAG:Ce. *Opt. Mater.*, 2017, Vol.71, pp.98–102. doi:10.1016/j.optmat.2016.05.016

16 Kucera M., Nikl M., Hanus M., Onderisinova Z. Gd3+ to Ce3+ energy transfer in multi-component GdLuAG and GdYAG garnet scintillators. *Phys. Stat. Solidi (RRL)*, 2013, Vol.7, pp. 571–574. doi:10.1002/pssr.201307256

17 Choe J.Y. Luminescence and compositional analysis of Y3Al5O12:Ce films fabricated by pulsed-laser deposition. *J. Mat. Res. Innovat.*, 2002, Vol.6, pp. 238-241. doi:10.1007/s10019-002-0204-4

18 Murai S., et al. Scattering-based hole burning in Y3Al5O12:Ce3+ monoliths with hierarchical porous structures prepared via the sol-gel route. *J. Phys. Chem*: *C*, 2011, Vol.115,pp. 17676–17681. doi:10.1021/jp204594c

19 Hakuta Y., et al. Continuous production of phosphor YAG:Tb nanoparticles by hydrothermal synthesis in supercritical water. *Materials Research*, 2003, Vol.38, pp. 1257-1265. doi:10.1016/S0025-5408(03)00088-6

20 Vasilica Ţucureanu, et al. Effect of process parameters on YAG:Ce phosphor properties obtained by co-precipitation method. *Ceramics Intern.,* 2020. Vol. 46, pp. 23802-23812. doi:10.1016/j.ceramint.2020.06.156

21 Huczko A. Fast combustion synthesis and characterization of YAG:Ce3+ garnet nanopowders. *Phys. Status Solidi B*, 2013, Vol.250, pp. 2702–2708. doi:10.1002/pssb.201300066

22 Lisitsyn V., et al. Luminescence of the tungsten-activated MgF2 ceramics synthesized under the electron beam. *Nuclear Inst. and Methods in Physics Research,* 2018, Vol.435, pp. 263–267. doi:10.1016/j.nimb.2017.11.012

23 Lisitsyn V.M., et al. YAG based phosphors, synthesized in a field of radiation. *IOP Conf. Series: Journal of Physics: Conf. Series,* 2018, Vol.1115, pp. 052007. doi:10.1088/1742-6596/1115/5/052007

24 Alpyssova G., Lisitsyn V.M., Karipbayev Zh.T. et al. Luminescence of cerium doped yttrium aluminumgarnet ceramics synthesized in the field of radiation flux. *Eurasian phys. tech. j*., 2021. Vol. 18, №3(37), pp. 37-42. doi 10.31489/2021No3/37-42

25 Hongling Shi, et al. Luminescence properties of YAG:Ce, Gd phosphors synthesized under vacuum condition and their white LED performances. *Optical Materials Express,* 2014, Vol.4(4), pp.649-655. doi:10.1364/OME.4.000649

26 Zorenko Y., Voznyak T., Gorbenko V., et al. Luminescence properties of Y3Al5O12:Ce nanoceramics. *J. Lumin.* 2011, Vol.131, pp. 17–21. doi:10.1016/j.jlumin.2010.08.015

27 Dorenbos P. 5d-level energies of Ce3+ and the crystalline environment. IV. Aluminates and «simple» oxides. *J. Lumin.* 2002, Vol.99, pp. 283–299. doi:10.1016/S0022-2313(02)00347-2

28 Munoz-Garcia A.B., Barandiaran Z., Seijo L. Antisite defects in Ce-doped YAG (Y3Al5O12): First-principles study on structures and 4f-5d transitions. *J. Mater. Chem.,* 2012, Vol. 22, pp. 19888–19897. doi:10.1039/C2JM34479C

29 He X., Liu X., Li R., et al. Effects of local structure of Ce3+ ions on luminescent properties of Y3Al5O12:Ce nanoparticles. *Sci. Rep.,* 2016, Vol.6, p. 22238. doi: 10.1038/srep22238

30 Lisitsyn V., Lisitsyna L., Tulegenova A., et al. Nanodefects in YAG:Ce-Based Phosphor Microcrystals. *Crystals*, 2019, Vol.9 p.476. doi:10.3390/cryst9090476.

Article accepted for publication 18.05.2023